Journal of Molecular Liquids 415 (2024) 126319

Contents lists available at ScienceDirect

Journal of Molecular Liquids

journal homepage: www.elsevier.com/locate/molliq

Aqueous dispersions of 'green' silver nanoparticles for eco-applications: Synthesis, structure and biosafety

Svitlana Dybkova [a,b], Olena Goncharuk [a,b], Liudmyla Rieznichenko [b], Konrad Terpiłowski [c], Larysa Borysenko [d], Tamara Gruzina [b], Kateryna Dybkova [b], Katarzyna Szewczuk-Karpisz [a,*]

[a] Institute of Agrophysics, Polish Academy of Sciences, Doświadczalna 4, 20-290 Lublin, Poland
[b] F.D. Ovcharenko Institute of Biocolloidal Chemistry, NAS of Ukraine, 42 Acad. Vernadskoho Ave., 03142 Kyiv, Ukraine
[c] Maria Curie-Sklodowska University, M. Curie-Sklodowska Sq. 3, 20031 Lublin, Poland
[d] Chuiko Institute of Surface Chemistry, NAS of Ukraine, 17 General Naumov Str., 03164 Kyiv, Ukraine

ARTICLE INFO

Keywords:
Silver nanoparticles
Green synthesis
Biocompatibility
Cytotoxicity
Genotoxicity

ABSTRACT

Sustainable agriculture requires the use of intelligent compounds with multifaceted effect on soil and plants. Such conditioners can be hydrogels enriched with nanoparticles, but only those synthesized using 'green chemistry' methods. Therefore, the main aim of the study was to synthesize and characterize innovative 'green' silver nanoparticles (AgNPs) for agricultural applications. AgNPs were created using water or alcohol extracts of eucalyptus (*Eucalyptus viminalis* Labill) and aloe (*Aloë arborescens* Mill) as well as tannin to reduce silver ions (Ag^{+}) to zero valent form (Ag^{0}). The synthesis was conducted under autoclave conditions or at room temperature, in the presence of potassium carbonate. The AgNPs characterization was performed by X-ray diffraction (XRD), scanning electron microscopy (SEM), transmission electron microscopy (TEM) and dynamic light scattering (DLS) method, whereas stability of the AgNPs suspensions under various conditions was estimated using turbidimetry. Biosafety of the formed species was determined based on genotoxicity (comet test) and cytotoxicity (study with crystal violet and MTT) assays. The obtained results confirmed the presence of zero valent silver phase in the nanoparticles and showed that their crystallite size was 14–24 nm, with different degrees of polydispersity depending on the synthesis conditions. Hydrodynamic diameter of AgNPs and their aggregates in the aqueous dispersions varied from 6 nm to 103 nm, and the smallest aggregation degree was noted for the nanoparticles synthesized using tannin. All synthesized nanoparticles were biosafe. Thus, they can be applied in agro-industrial processes without damaging the environment.

1. Introduction

The use of nanotechnology in agriculture, where silver nanoparticles (AgNPs) are emerging as a promising agent for improving plant vegetation, has attracted great interest in recent years. AgNPs possess unique physicochemical properties that make them suitable for various applications, including improving plant development and resistance to environmental stressors [1–3]. Nanoparticles are prepared using various techniques, including chemical, physical and biological ones [4–7], but eco-friendly synthesis using plant extracts should be used most often for safety reasons [7–10]. Characterization techniques, including transmission electron microscopy (TEM), scanning electron microscopy (SEM), X-ray diffraction (XRD), Fourier-transform infrared spectroscopy (FTIR) and turbidimetry, can be employed to determine size, shape and stability of the obtained metallic nanoparticles [11].

Silver nanoparticles exhibit multidirectional action mechanisms in

Abbreviations: AgNPs, silver nanoparticles; CC_{50}, 50 % cytotoxicity concentrations (CC50) is the concentration of test compounds required to reduce cell viability by 50 %; CV, Crystal Violet; DLS, Dynamic Light Scattering; DMEM/F12, Dulbecco's Modified Eagle Medium F12; DNA, Deoxyribonucleic acid; EDTA, Ethylenediaminetetraacetic acid; FSC, Fetal Calf Serum; HRTEM, High-Resolution Transmission Electron Microscopy; I_{DNA}, "DNA- comets" index; IMA, index of metabolic activity; MTT, MTT assay, a colorimetric assay for assessing cell metabolic activity using 3-(4,5-dimethylthiazol-2-yl)-2,5-diphenyltetrazolium bromide; MA104, MA-104 Clone 1 is an epithelial cell from the kidney of an African green monkey; PDS_I, Particle Size Distribution by Intensity; SEM, Scanning Electron Microscopy; TSI, Turbiscan Stability Index; XRD, X-ray Diffraction.

* Corresponding author.
E-mail address: k.szewczuk-karpisz@ipan.lublin.pl (K. Szewczuk-Karpisz).

https://doi.org/10.1016/j.molliq.2024.126319
Received 13 June 2024; Received in revised form 16 September 2024; Accepted 19 October 2024
Available online 24 October 2024

Table 1
The composition of the synthesized AgNPs dispersions [26–29].

Sample name	Plant extracts	Main active ingredients	Concentration of Ag, mg/mL
AgNP#1	alcohol extract of eucalyptus *Eucalyptus viminalis* Labill	essential oils, eucalyptol, pineol, citriodorol, tannins, flavonoids, aldehydes, monoterpenes, resins	0.8
AgNP#2	water extract of eucalyptus *Eucalyptus viminalis* Labill		0.8
AgNP#3	tannin reagent	Tannin	0.8
AgNP#4	water aloe extract (*Aloe arborescens* Mill)	vitamins (A, B1, B2, B6, B9, B12, C, E), tannins, catechins, carotenoids, flavonoids, enzymes	0.43

plants. They penetrate plant tissues and affect various physiological and biochemical processes. So far, AgNPs were shown to enhance nutrient uptake, stimulate seed germination and promote root and shoot growth [12]. They can also enhance photosynthetic efficiency, increase chlorophyll content and thus improve overall biomass production [13,14]. AgNPs modulate the activity of antioxidant enzymes, thereby alleviating oxidative stress in plants exposed to unfavorable environmental conditions [15–18]. When plants face various environmental stressors like drought, AgNPs regulate water balance and increase plant ability to withstand adverse conditions [19]. Therefore, silver nanoparticles can be considered as suitable for agriculture practice, especially in the regions prone to environmental challenges.

Despite potential benefits of AgNPs, their use always raises concerns about their environmental impact and safety. This is extremely important to evaluate the risk–benefit balance and establish guidelines for the responsible use of such materials in agriculture. Previous studies were aimed at investigating the potential toxicity of AgNPs to non-target organisms, soil microbiota and aquatic ecosystems [20–22]. In this study, silver nanparticles synthesized using water or alcohol extracts of eucalyptus and aloe as well as tannin as reducing agents were examined towards their structural properties, stability and biosafety. Ecotoxicity study included cytotoxicity and genotoxicity assays. The cytotoxicity test is one of the most important methods of *in vitro* biological analysis, used usually to assess the safety of substances in relation to the cells of various tissues. The methods with crystal violet or MTT enable determination of several parameters like cell metabolism, membrane integrity, mitochondrial activity, cell proliferation using only one cell sample. Live and dead cells are distinguished, which indicates the level of their growth inhibition [23,24]. On the other hand, the *in vitro* tests of genotoxicity are performed to detect primary DNA damage. Comet assay performing under the alkaline conditions is a simple and sensitive method for assessing DNA mutations and transformation at the level of one cell. It is capable of detecting double-stranded and single-stranded DNA breaks and areas of incomplete excision repair [25]. The performed experiments were devoted to establishing the relationship between the synthesis conditions, the structure of the obtained silver nanoparticles and their ecotoxicity for the further AgNPs application as components of hydrogel materials or separately used bio-fertilizers.

2. Experimental

2.1. Reagents

The following reagents were used for the synthesis of AgNPs: silver nitrate ($AgNO_3$, BioXtra, >99 %, Sigma Aldrich), potassium carbonate (K_2CO_3, 99.995 % trace metals basis, Sigma Aldrich), alcohol tincture (1:5) of eucalyptus leaves (*Eucalyptus viminalis* Labill) prepared using 70 % ethanol (Ternofarm, Ukraine), water extract of eucalyptus leaves (*Eucalyptus viminalis* Labill), tannin (ACS reagent, Sigma Aldrich), water extract of aloe (*Aloe arborescens* Mill). To prepare water aloe extract, 25 g washed leaves were cut and boiled (100 °C) in 100 mL of distilled water. An water extract of eucalyptus leaves was obtained by infusing 6 g of dry plant material in 200 mL of distilled water at a temperature of 70 °C for 45 min. The extracts were separated from the plant material by

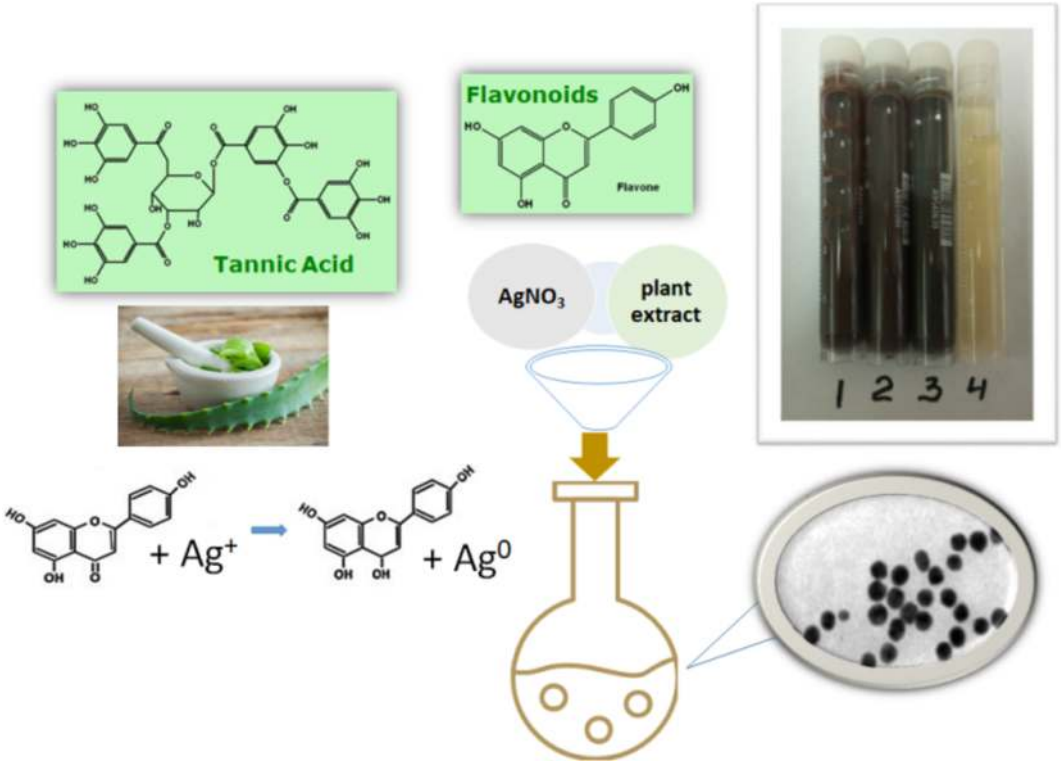

Fig. 1. Scheme of silver nanoparticles synthesis.

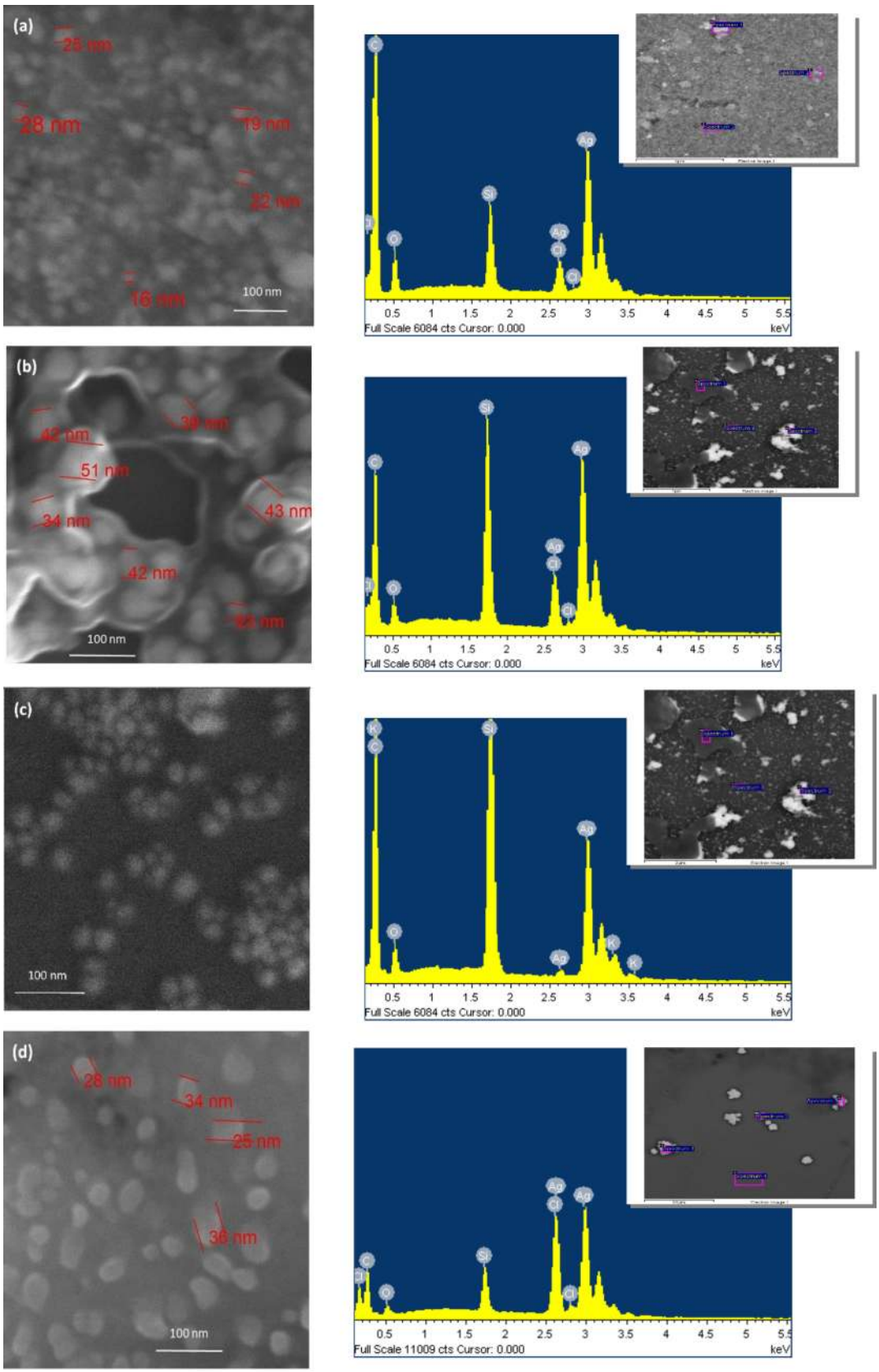

Fig. 2. SEM images of silver nanoparticles: (a) AgNP#1, (b) AgNP#2, (c) AgNP#3, (d) AgNP#4, as well as the results of their EDX analyses.

Table 2
The elemental composition of preparations according to the SEM/EDX data.

Sample	C wt.%	O wt.%	Si* wt.%	Cl wt.%	Ag wt.%
AgNP#1	42.33	5.71	4.11	2.29	45.56
AgNP#2	24.52	3.46	15.46	3.21	53.35
AgNP#3	33.08	3.56	16.99	1.92	44.45
AgNP#4	14.00	2.40	13.07	15.88	54.65

* Si is a substrate material for the SEM/EDX study.

filtering through the Whatman N1 filter paper.

2.2. Methods

2.2.1. Synthesis of AgNPs

AgNPs were synthesized by reduction of silver nitrate using plant water and alcohol extracts as reducing agents (Table 1, Fig. 1). AgNP#1 (Ag concentration equal to 0.8 mg/mL) was synthesized using alcohol extract of eucalyptus leaves in the presence of potassium carbonate. 80 mL of 9×10^{-3} M $AgNO_3$ solution was mixed with 15 mL of 15×10^{-3} M K_2CO_3 solution, and then 5 mL of alcohol extract of eucalyptus leaves was added. The received mixture (pH 5.2) was autoclaved under conditions: temperature 121 °C, pressure 1.04 atm, time 15 min. AgNP#2 (Ag concentration equal to 0.8 mg/mL) was obtained using water extract of eucalyptus leaves. 50 mL of 15×10^{-3} M $AgNO_3$ solution was mixed with 50 mL of water extract, and the prepared mixture (pH 4.4) was autoclaved under conditions: temperature 121 °C, pressure 1.04 atm, time 15 min. AgNP#3 (Ag concentration equal to 0.8 mg/mL) was synthesized using tannin. 50 mL of 15×10^{-3} M of silver nitrate was mixed with 25 mL 0.07 % tannin solution in the presence of 25 mL of 13×10^{-3} M potassium carbonate solution (pH 5.9). The reaction conditions were: temperature 121 °C, pressure 1.04 atm, time 15 min. AgNP#4 (Ag concentration equal to 0.43 mg/mL) was synthesized using water aloe extract. 2.5 mL of 30 % ammonia solution was added to 5 mL of 10^{-2} M $AgNO_3$ solution followed by the addition of 5 mL of aloe extract making up the final volume to 50 mL with water (pH 8.4), at room temperature [26].

2.2.2. Scanning electron microscopy (SEM)

The morphological analysis of AgNPs was carried out using transmission electron microscopy (TEM) and scanning electron microscopy (SEM) methods. SEM was performed using a TESCAN Mira 3 LMU microscope equipped with an EDS microanalyzer OXFORD X-MAX detector. The experiments were conducted using the samples sprayed with a conductive Au layer at an accelerating voltage of 15 keV.

TEM images were captured using a Tecnai G2 T20 X-TWIN (FEI Company, USA) apparatus operating at a voltage of 200 kV with electron source. The samples were prepared by pipetting 5 μL of the sample onto carbon-coated copper TEM grids, which were allowed to dry at room temperature.

An open-source image processing software ImageJ 1.53a, Java 1.8.0_112 [64-bit] was used to analyze the size distributions from TEM images. The size (diameter) distributions of AgNPs were generated by measuring a minimum of 200 particle's diameters in the TEM and SEM images.

2.2.3. X-ray diffraction (XRD)

X-ray diffraction (XRD) patterns of the samples were recorded using a DRON-3M diffractometer with the CuKα radiation and nickel filter. The measurements were performed in the mode of reflected rays and the Bragg–Brentano geometry of focusing. The data were collected in the angle range of 5–70° with a step of 0.05°. Phase identification was performed by using the PDF-2 X-ray database [30]. The average crystallite size was determined from 38.14° X-ray line broadening using the Scherrer equation [31]:

$$D = \frac{0.9\lambda}{\beta/\cos\theta} \quad (1)$$

where D is the average crystalline size (nm), λ is the X-ray wavelength used (0.15418 nm), β is the angular line width at half maximum intensity (radians) and θ is the Bragg's angle (degrees).

2.2.4. Dynamic light scattering (DLS)

Particle size distribution (PSD_I) was studied using a Zetasizer Nano ZS (Malvern Instruments) apparatus with a universal dip cell (ZEN1002) [32]. The samples for the PSD measurement were prepared as follows: the synthesized aqueous dispersion of AgNPs was diluted 100 times (AgNP#1, AgNP#2, AgNP#3) or 50 times (AgNP#4) and sonicated for 3 min at the frequency 22 kHz in distilled water. Then it was kept for 1 h, and the PSD measurement was performed. This allowed to calculate average effective diameter (D_{ef}, also known as hydrodynamic diameter) of AgNPs.

2.2.5. Turbidimetric method

The stability measurements of the AgNP suspensions, under different physicochemical conditions, were performed using a Turbiscan Lab Expert with a TLAb Cooler cooling module (Formulaction, France). To determine the stability, the AgNP suspensions were diluted 10 times. The applied apparatus had an electroluminescence diode emitting a collimated light beam ($\lambda = 880$ nm), which passed through the dispersion. During the measurement, two synchronized detectors (transmission and backscattering) recorded light passing through a probe at the angle of 0° (in relation to the incident light direction) and the light scattered at the angle of 135°. The results were presented in the form of curves, which showed the intensities of transmission and scattering as a function of time [33]. The samples stability was also estimated using the Turbiscan Stability Index (TSI). This parameter took into account all single measurements during experiments, and the TSI value was obtained from their averaging. This index was calculated with the special computer program Turbiscan Easy Soft using the following formula:

$$TSI = \sqrt{\frac{\sum_{i=1}^{n}(x_i - x_{BS})^2}{n-1}} \quad (2)$$

where x_i is the average transmission/backscattering for each minute of measurement, x_{BS} is the average x_i and n is the number of scans (repetitions of single measurement during the total time of the experiment). The TSI values change in the range of 0 (very stable system) to 100 (extremely unstable system).

2.2.6. Study of cytotoxicity

To determine the cell viability after their contact with the AgNP samples, two *in vitro* tests were conducted: the first with crystal violet (CV) and the second, with MTT (3-(4,5-dimethylthiazol-2-yl)-2,5-diphenyltetrazolium bromide tetrazole) [23,24]. For the cytotoxicity tests a monolayer culture of MA104 (MA-104 Clone 1, ATCC® CRL-2378.1) and cells in the logarithmic growth phase were used. Cells were removed from the surface of the vials using a trypsin-EDTA solution, resuspended in a nutrient medium, and their concentration in the suspension was adjusted to 5×10^5 cells/mL. 0.1 mL of the cell suspension was added to 96-well flat-bottom plates in the DMEM/F12 nutrient medium with the addition of 10 % fetal calf serum (FSC) and an antibiotic–antimycotic and incubated in a thermostat with a constant level of carbon dioxide (CO_2, 5 %) at 37 °C for 24 h until a monolayer of cells was formed.

During the study with MMT, the obtained dilutions of AgNPs samples were *ex tempore* added at the ratio of 1:10 to the nutrient medium with the cells formed a monolayer in the 96-well plates. Such prepared plates were incubated at 37 °C for 24 h. Then, the medium was removed and

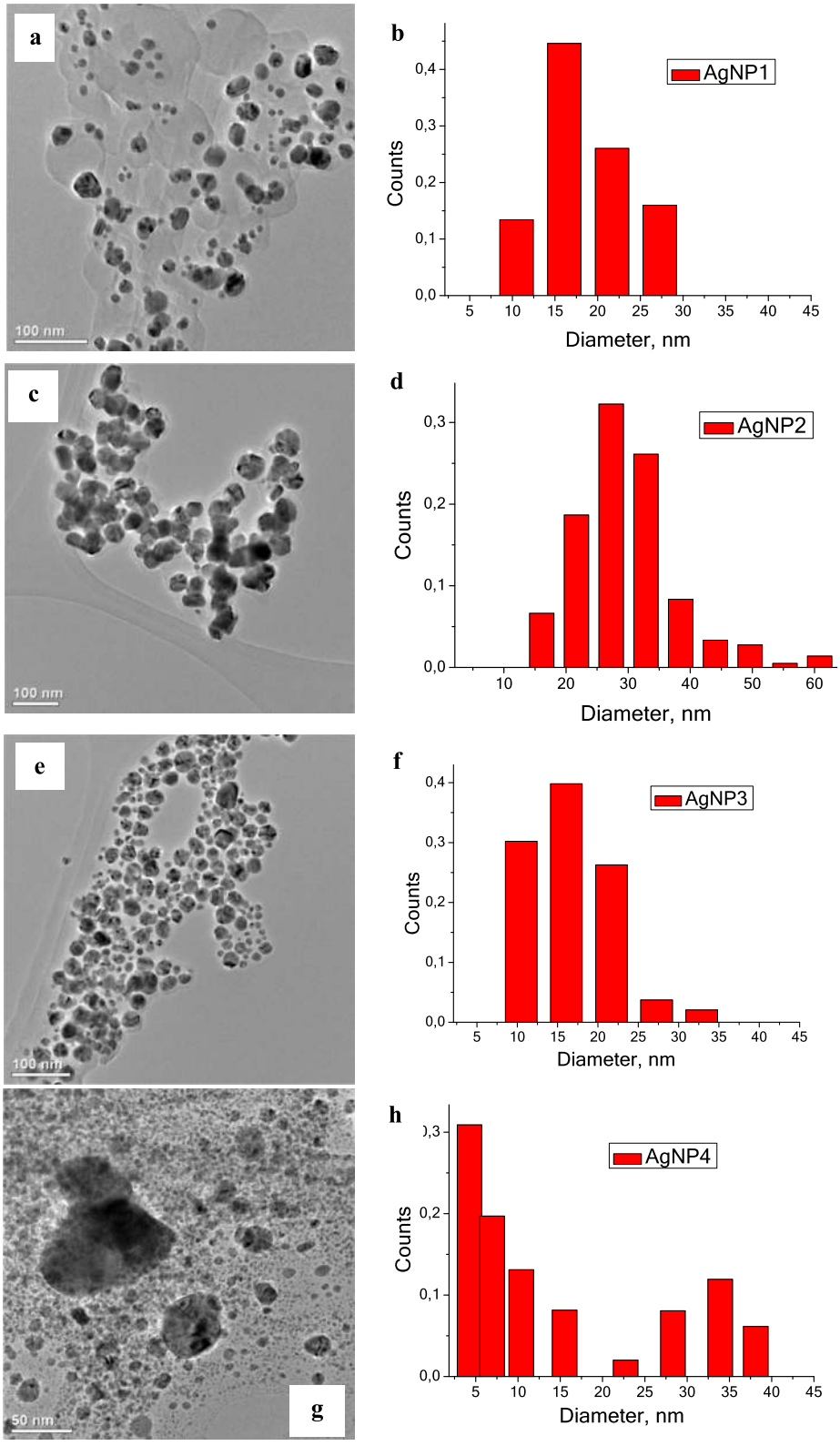

Fig. 3. TEM images of silver nanoparticles and particle size distribution calculated from them: (a, b) AgNP#1; (c, d) AgNP#2; (e, f) AgNP#3; (g, h) AgNP#4.

50 μL of the working solution of the MTT reagent (0.1 mg/mL in a phosphate-buffered saline (PBS)) was added to the cells in each well and incubated again in a thermostat for 2 h. After this time, the supernatant was removed and a lysing solution containing dimethyl sulfoxide (DMSO) was added to the cells. The optical density of wells with a solution of diformazan in DMSO was measured at a wavelength of 492 nm using a LabSystem Multiscan vertical axis photometer.

Cytotoxicity testing by the crystal violet was performed according to the following protocol. After incubation of cells with the AgNPs samples, carried out in the same way as during the MTT test, the medium was removed from the plate, and 0.5 % solution of crystal violet (Sigma-Aldrich, USA) in 30 % ethanol was added to the plate. Then, the cells

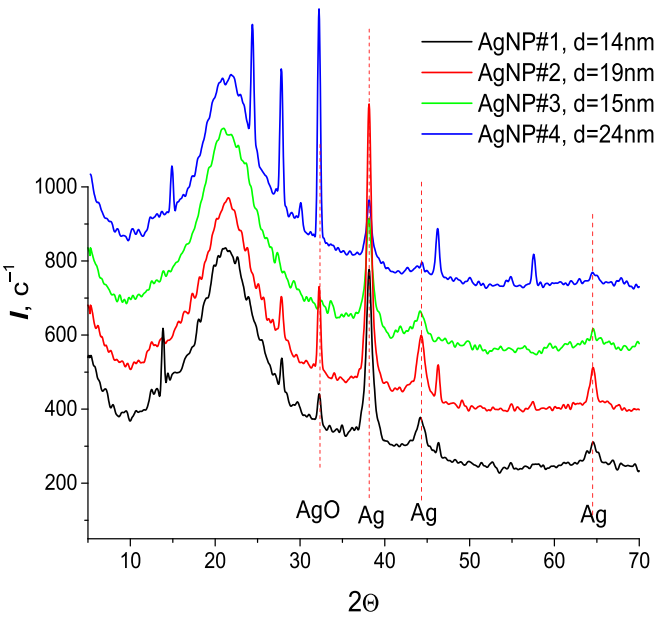

Fig. 4. XRD patterns of the synthesized AgNPs.

were stained for 10 min at room temperature, the dye was removed, and the cells were carefully washed with water to completely remove unbound dye. After drying the plates, the optical absorption of the wells was measured at a wavelength of 540 nm.

The number of living cells (N) for both used methods was calculated according to the standard formula:

$$N = \left(OD_{\exp}/OD_{cont}\right)\cdot 100\% \quad (3)$$

where OD_{exp} is the optical density of the solution in the experimental wells (treated with AgNPs), and OD_{cont} is the optical density of the solution in the wells of the intact control.

The obtained values were processed by calculating the percentage of metabolically active (MTT assay) and adherent (crystal violet assay) cells in relation to the control cells (not treated with AgNP dispersion), for which the corresponding optical density values were taken as 100 %. The CC_{50} value, i.e., the cytotoxic concentration that causes 50 % destruction of the cell monolayer, was calculated. Also, the index of metabolic activity (IMA) of cells, that is, the ratio of the percentage of metabolically active cells (according to the MTT test) to the percentage of adhered cells (according to the crystal violet test), was determined. The IMA of cells is an integral indicator that allows to analyze the depth of metabolic changes in the cells induced by AgNPs. For the control intact cells, the IMA is 1.0. An indicator above 1.0 shows that the activity of cells is greater than their total number. Conversely, a decrease in the indicator below 1.0 indicates reduced metabolic activity of cells in relation to their total number in the well. Provided that the IMA is 1.0, the number of metabolically active cells corresponds to the number of adherent cells. The response of cells to a toxic stimulus can be accompanied by their hyperactivation or a decrease in the number of cells without hyperactivation. The study of data and parameters was statistically processed and presented as the median with the interquartile range AUC: Me (LQ–UQ), where Me = median (50 % percentile), LQ = 25 % percentile, and UQ = 75 % percentile. Statistical calculations were performed using the Stat Plus Pro 5.9.8 software and STATISTICA v.10 (Experimental Data Analysis System, StatSoft, Inc. 2011).

2.2.7. Study of genotoxicity

The genotoxicity of the AgNP samples was assessed *in vitro* by the DNA-comet method under the alkaline conditions according to the technique described in the papers [25,34,35]. In these tests MA104 (MA-104 Clone 1, ATCC® CRL-2378.1) cell culture was used. As a positive control there a test culture of cells in the amount of 5×10^5 cells/mL, treated with a mutagen – the chemical compound of the positive control (N-nitrosomethylurea, 1×10^{-3} M), was applied, whereas as the negative control, the solvent – sterile distilled water. After 24 h of exposure of the formed MA104 cells monolayer (created as described in the previous subchapter) with the investigated AgNPs samples at various concentrations, a possible genotoxic effect was determined. The micropreparations were formed on the microscopic slides with the agarose plate (1 % agarose gel of normal molten agarose ($T_{mel} < 65$ °C), on which 60 μL of treated cell suspension and 60 μL of 0.5 % agarose gel were spread. At the next stage, the slides with the immobilized in agarose preparations were immersed in the freshly prepared cold lysis solution (10 mM Tris-HCl (pH 10.0), 2.5 M NaCl, 100 mM EDTA-Na_2, 1 % Triton X-100 and 10 % DMSO) for 3 h at 4 °C. When the lysis procedure was over, the slides were placed in a horizontal gel electrophoresis tank filled with the fresh cold electrophoresis solution (300 mM NaOH, 1 mM EDTA-Na_2, pH > 13.0, 4 °C) for the alkaline DNA denaturation (20 min under the switched off apparatus). The distribution of denatured DNA was conducted by gel-electrophoresis during 20–30 min under the field strength 1 V/cm and the current intensity not more than 250 mA. The preparations were fixed using the 70 % ethanol solution for 15 min when electrophoresis was over. The obtained micropreparations were stained by the acridine orange fluorescent dye within 30 min, and 'DNA-comets' were visualized using a fluorescent microscope 'LUMAM R8′ (exciting filter 490 nm, dichroic mirror 510, reflective filter 530 nm, magnification X200–400). The analysis of 'DNA-comets' were performed visually. For this purpose, the 'DNA-comets' were divided into five conditional types (Fig. S1) with a corresponding number from 0 to 4 for each. For each micropreparation, 200 'DNA-comets' without 'tails' overlays were analyzed. The degree of DNA damage was expressed as the 'DNA-comets' index (I_{DNA}) calculated according to the formula:

$$I_{DNA} = (0\cdot n_0 + 1\cdot n_1 + 2\cdot n_2 + 3\cdot n_3 + 4\cdot n_4)/\Sigma \quad (4)$$

where: n_0-n_4 – the number of "DNA-comets" of each type (Fig. S1), Σ – the sum of 'DNA-comets'.

The experiments were performed in two parallels. The statistical analysis of the results was made comparing the indices of DNA damage in the experimental and control groups. The data of two replications were combined and the average parameter for each group was calculated. Statistically significant high indices of DNA damage (data close to the positive control) serve as criteria of a positive result. The differences $p < 0.05$ were considered significant.

3. Results and discussion

3.1. SEM and TEM morphology analysis of AgNPs

The SEM images, presented in Fig. 2, indicated that the particle shape of AgNP#1 and AgNP#3 was close to the spherical one. However, the irregular particle shape was observed for the AgNP#2 and AgNP#4 samples. The particles in the AgNP#1 and AgNP#2 samples are aggregated, while the AgNP#3 sample was characterized by the smallest aggregation and polydispersity.

The energy dispersive X-ray analysis (SEM/EDX) (Fig. 2, Table 2) confirmed the formation of AgNPs – the strong signal in a silver region was noticed. Generally, metallic silver nanocrystals show typical optical absorption peak at approximately 2.983 keV due to the surface plasmon resonance.

In Fig. 3, the TEM images and the particle size distribution calculated from them for four synthesized samples of AgNPs are presented. It can be seen that a narrow monomodal size distribution and close sizes of silver nanoparticles were observed for AgNP#1 and AgNP#3. The diameter of the particles for these samples according to TEM was in the range from 10 to 30–35 nm with a maximum of about 15–17 nm. The particle shape

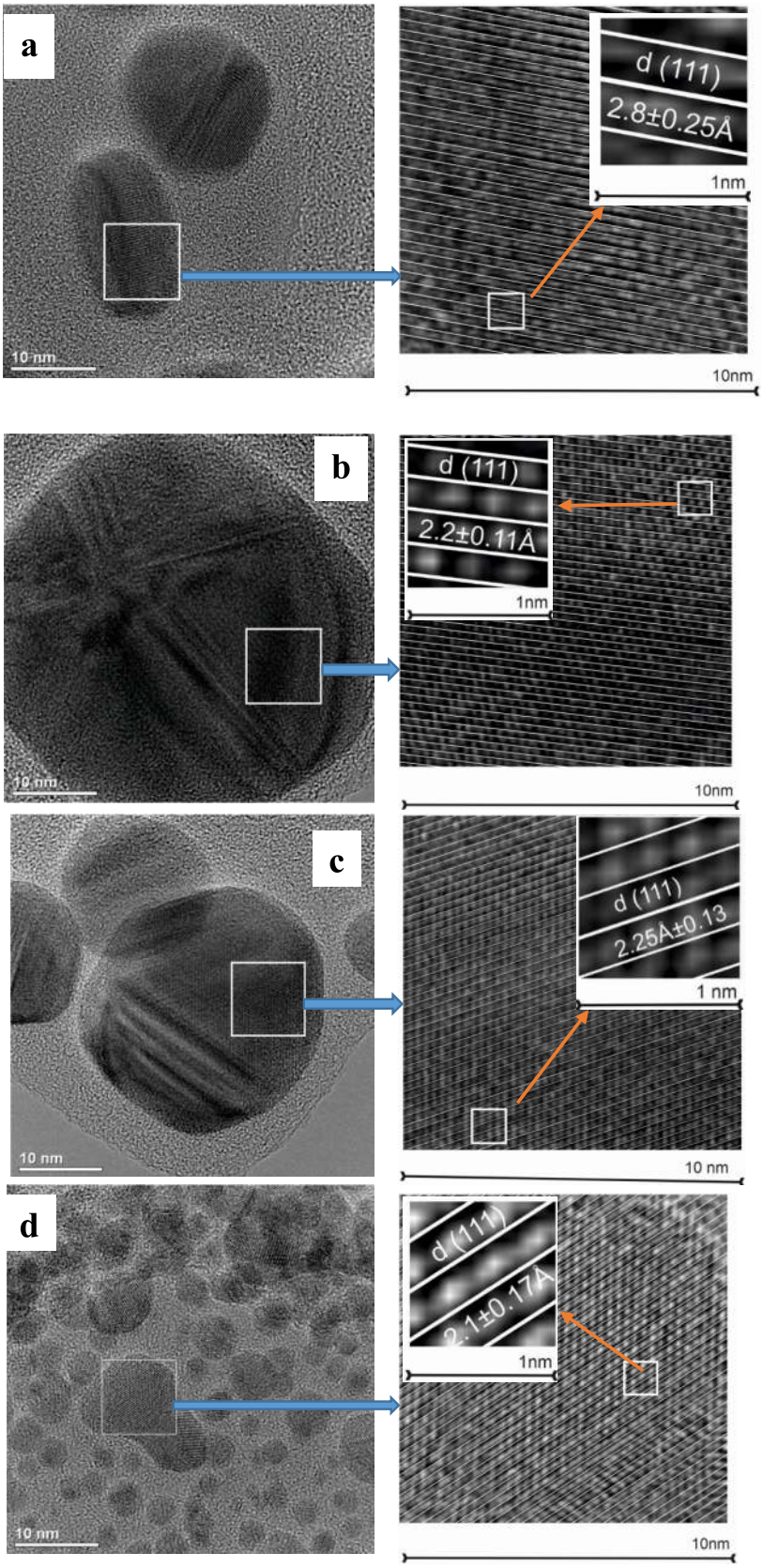

Fig. 5. Representative HRTEM micrographs of AgNPs and the calculated interplanar spaces corresponding to face centered cubic structure: a – AgNP#1; b – AgNP#2; c – AgNP#3; d – AgNP#4.

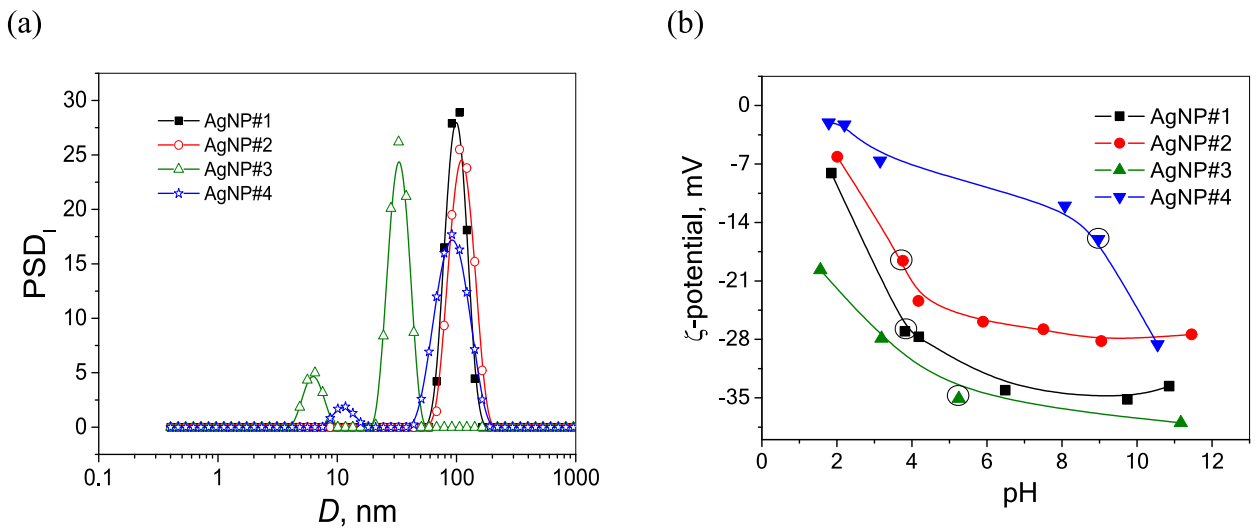

Fig. 6. (a) PSD of AgNPs in the aqueous dispersions measured by the DLS technique, and (b) zeta potential of AgNPs as a function of suspension pH value.

was close to spherical, but not ideal. For the AgNP#2 sample, the particle distribution was wider and corresponded to a larger diameter (from 15 to 60 nm, with a maximum around 28 nm). In the AgNP#4 sample, a very large proportion of small silver nanoparticles, whose diameter is less than 10 nm, was observed, but AgNPs with a larger diameter (up to 30–45 nm) and aggregates of nanoparticles were also observed.

Comparing TEM and SEM images, it can be concluded that for the samples of AgNP#1, AgNP#2, and AgNP#3, mainly individual, spherical nanosilver particles were observed, while for AgNP#4, the aggregates of irregular shape were noted.

3.2. TEM and X-ray phase analysis of crystalline structure of AgNPs

X-ray diffraction (XRD) patterns were used to determine the crystal structure of AgNPs by comparing the observed diffraction peaks with known reference patterns (Fig. 4). For silver, the cubic and hexagonal crystal lattices had distinct diffraction patterns due to their different crystal structures.

As it was mentioned above, silver typically crystallizes in a face-centered cubic (FCC) structure. The Miller indices corresponding to the main diffraction peaks for FCC silver are: (111), (200), (220), (311), (222) [36]. The interplanar spacings (d-spacings) and peak intensities will follow the FCC structure's selection rules, and these peaks will appear at specific angles based on Bragg's Law. Hexagonal crystal lattice of silver (HCP – Hexagonal Close-Packed) is less common for bulk silver, but the hexagonal close-packed (HCP) structure can sometimes be observed in nanostructured or stressed silver particles. The Miller indices for HCP structures, that correspond to XRD peaks, include: (100), (002), (101), (102), (110), (103), (112) [37]. The pattern for HCP silver will show different d-spacings and peak positions compared to FCC silver. FCC silver typically shows strong peaks at lower angles for (111), (200) and (220) reflections. The (111) peak is usually the most intense and peaks are evenly spaced in terms of $\sin^2\theta$. For HCP silver peaks appear at different angles due to the different crystal geometry. The intensity distribution will differ, with possible strong reflections from planes such as (100), (002) or (101). The peaks will not follow the same spacing or intensity patterns as in the FCC structure. Thus, to identify whether an XRD pattern corresponds to cubic or hexagonal silver, the observed peak positions (angles) and intensities with the expected patterns for FCC and HCP structures should be compared. FCC silver typically shows major XRD peaks around 38.1° (111), 44.3° (200), 64.5° (220), 77.5° (311) and 81.7° (222).

Besides crystalline nature of AgNPs, XRD analyses can indicate the overall oxidation state of Ag. In the examined AgNPs samples, the presence of both metallic and oxidized silver was confirmed (Fig. 4). The prominent peaks at $2\theta = 38.14°$, 44.34°, 64.46° represented the (111), (200) and (220) Bragg's reflections of the FCC structure of silver, respectively [30]. The minor diffraction peaks at $2\theta = 32.56°$ (202) and 46.17° (132) indicated the presence of AgO in the AgNP samples [31]. The low intensity peaks observed for AgO indicated that the synthesized samples contained mostly Ag^0 nanoparticles with the AgO trace. The crystallite sizes of synthesized silver nanoparticles calculated according to the Scherrer equation varied in the range of 14–24 nm.

The HRTEM allowed to obtain images of AgNPs with a very high resolution enough to observe their atomic structure. HRTEM images showed interference patterns (fringes) resulting from the interaction of electrons with the crystal lattice. By measuring the distances between these fringes, it was possible to determine the interplanar distances and compare them with the theoretical values for the corresponding crystal planes. For bulk silver, functionally centered cubic (FCC) crystal structure is the most typical, which is characterized by distinct, regular lattice fringes (interference fringes) with high periodicity and the most noticeable planes: (111), (200), (220), (311) with interplanar distances $d_{111} = 0.24$ nm, $d_{200} = 0.21$ nm, $d_{220} = 0.14$ nm, $d_{311} = 0.12$ nm. Hexagonal close-packed (HCP) is not characteristic of bulk silver. Some researchers reported the HCP structure in silver nanoparticles, which was usually formed under certain synthesis conditions or after heat treatment [37].

For this structure, a less regular order was observed compared to FCC, since the layers were repeated through one (ABAB…), and the most prominent planes were (100), (002), (101) with interplanar distances $d_{100} = 0.23$ nm, $d_{002} = 0.21$ nm, $d_{101} = 0.19$ nm. In practice, silver most commonly crystallizes in the FCC structure, and the HCP structure would be highly unusual for silver under normal conditions. Also, some authors described the obtained Multiple Twinned Particles (MTPs), which were also characteristic for silver nanoparticles when synthesized under conditions that favour twin growth [38]. These are structures, where several FCC crystals are joined at certain angles, forming complex polyhedral shapes, and their images contain areas with different orientations of crystal lattices and reflect twin boundaries, which appear as interruptions or changes in the direction of lattice fringes. Usually, each twinning corresponds to an FCC structure, so the interplanar distances are the same as in FCC. Such structures of fused crystallites can be seen on the HRTEM image of AgNP#2 (Fig. 5b). The interplanar distances (d-spacings) given in Fig. 5 for the four samples of AgNP can be compared to the known d-spacings for silver's common crystal structures, particularly the FCC structure. It is known that d-spacings for FCC of silver [36] is: (111) plane $d_{111} \approx 2.359$ Å; (200) plane $d_{200} \approx 2.043$ Å; (220)

Table 3
Parameters characterizing stability of aqueous AgNP dispersions.

Sample	Dispersion medium (solvent)	D_{ef}	ζ potential, mV	TSI 3 days	TSI 7 day	TSI 20 days
AgNP#1	initial sample diluted 10 times with distilled water (pH 3.9)	215.6 nm	−28.3	4.9	12.6	14.5
	0.1 M solution NaCl	2.1 μm	−17.5	35.3	64.3	69.6
	0.1 M solution $CaCl_2$	2.0 μm	−6.3	46.5	37.9	44.7
	0.1 M solution $AlCl_3$	2.8 μm	+9.5	47.8	40.5	58.0
	solution HCl (pH 3)	716 nm	−13.5	26.4	30.3	43.8
	solution HCl + NaCl (pH 10)	3.2 μm	−6.9	55.7	45.6	65.7
	solution NaOH (pH 10)	138.0 nm	−35.0	9.8	11.8	16.4
	solution NaOH + NaCl (pH 10)	241.2 nm	−31.5	8.9	9.2	24.8
AgNP#2	initial sample diluted 10 times with distilled water (pH 3.8)	293.4 nm	−19.2	25.2	39.9	54.7
	0.1 M solution NaCl	328 nm	−12.1	35.0	36.2	44.8
	0.1 M solution $CaCl_2$	1.31 μm	−5.71	43.3	39.5	57.1
	0.1 M solution $AlCl_3$	1.25 μm	+6.09	64.5	58.1	72.0
	solution HCl (pH 3)	445.3 nm	−16.2	26.5	46.0	59.3
	solution HCl + NaCl (pH 3)	756.4 nm	−10.1	23.8	19.0	26.1
	solution NaOH (pH 10)	236.3 nm	−31.5	17.5	33.2	47.7
	solution NaOH + NaCl (pH 10)	319.2 nm	−21.8	37.5	41.5	52.8
AgNP#3	initial sample diluted 10 times with distilled water (pH 5.2)	46.2 nm	−35.2	8.8	18.5	36.3
	0.1 M solution NaCl	801.6 nm	−33.5	67.5	60.4	73.7
	0.1 M solution $CaCl_2$	782.0 nm	−7.7	62.8	54.6	70.1
	0.1 M solution $AlCl_3$	888.3 nm	+10.9	63.5	56.1	69.8
	solution HCl (pH 3)	132.2 nm	−22.0	17.8	23.9	29.8
	solution NaOH (pH 10)	75.3 nm	−41.7	6.2	14.7	32.4
	solution NaOH + NaCl (pH 10)	516.7 nm	−32.8	68.1	63.2	71.8
AgNP#4	initial sample diluted 10 times with distilled water (pH 8.9)	191 nm	−17.5	3.4	3.9	4.1
	0.1 M solution NaCl	235.3 nm	−18.6	9.4	10.1	10.7
	0.1 M solution $CaCl_2$	3.1 μm	+3.2	11.3	11.5	11.9
	0.1 M solution $AlCl_3$	218 nm	+25.2	29.1	24.8	31.3
	solution HCl (pH 1.7)	402 nm	−2.04	33.2	39.4	50.4
	solution HCl + NaCl (pH 1.7)	899 nm	−0.73	59.9	14.0	15.5
	solution NaOH (pH 11)	114.3 nm	−19.4	6.4	8.0	8.8

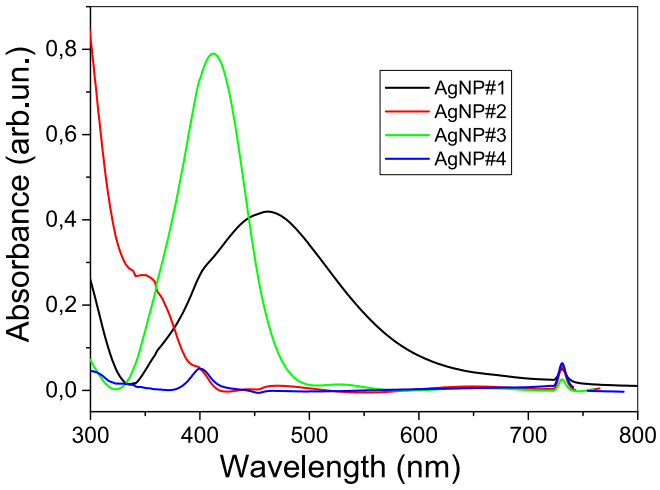

Fig. 7. UV–Vis spectra of the AgNPs samples.

plane $d_{220} \approx 1.443$ Å; (311) plane: $d_{311} \approx 1.232$ Å. The calculated interplanar distances for the samples of AgNP#2 (Fig. 5b) and AgNP#3 (Fig. 5c) were 2.2 and 2.25 Å, respectively. They were close to d_{111} of FCC of silver, though they were slightly smaller than the typical (2.359 Å). It was possible that the small discrepancy could be due to slight variations in measurement or strain in the nanoparticles. For the sample of AgNP#4, the calculated d-spacing was 2.1 Å. That value was close to the d_{200} value for the FCC structure. At the same time for the sample of AgNP#1, d-spacing was 2.8 Å, that was larger than typical values for the FCC silver. It did not correspond to any of the standard low-index planes in the FCC silver. This could indicate a different crystallographic structure, a high-index plane in a different structure or even the presence of a different phase of silver (e.g., a hexagonal or another possible metastable structure, though these are rare for silver).

In summary, most of the samples appear to be consistent with the FCC crystal structure, while AgNP#1 might suggest a different or distorted structure.

3.3. Characterization of aqueous AgNPs dispersions by DLS and UV–Vis spectroscopy

Particle size distribution with respect to the intensity of scattered light (PDS_I) was measured for AgNPs using dynamic light scattering (DLS) [39]. AgNPs were found to be polydispersed and the maximum was 101–103 nm for AgNP#1 and AgNP#2, 30 nm for AgNP#3 and 93 nm for AgNP#4 (Fig. 6a, Table 3). For the AgNP#3 and AgNP#4 samples, a bimodal size distribution was observed, where the first maximum corresponded to the smallest hydrodynamic diameter of particles (about 6 nm for AgNP#3 and 10 nm for AgNP#4), and the second maximum corresponded to the nanoparticles with a larger diameter (30 nm for AgNP#3). These results were consistent with the SEM data.

The zeta potential (ζ potential) represents the electrical potential at the slipping plane of particle in colloidal dispersion. It is a key indicator of the stability of colloidal systems, including dispersions of silver nanoparticles. A high absolute value of ζ-potential (whether negative or positive) typically implies strong electrostatic repulsion between particles, leading to a stable dispersion. Conversely, a decrease in the magnitude of zeta potential (especially towards zero) indicates a reduction in electrostatic repulsion, increasing the likelihood of particle aggregation and sedimentation. Fig. 6b shows the dependence of zeta potential on pH for the studied samples of silver nanoparticles. In the entire pH range, the zeta potential had negative values, its absolute value increases with increasing pH. According to literature data [40], the dispersions for which the absolute value of the zeta potential reaches more than 30 mV are considered stable, in this case the determining

Table 4
Viability (% living cells) of eukaryotic cells line MA-104 in the MTT and crystal violet assays.

Sample	Concentration of NP'sμg/mL	% living cells in MTT test	CC_{50}, μg/ml in MTT test, μg/mL	% living cells in crystal violet assay	CC_{50}, μg/ml in crystal violet assay	Index of the cell's metabolic activity
AgNP#1	80	44	19.1	14	17.6	3.04
	60	38	[18.5–19.3]	12	[15.6–18.0]	3.13
	40	36		11		3.45
	30	36		10		3.55
	20	**44**		**22**		2.03
	15	**75**		**81**		**0.93**
	10	82		95		0.87
	7.5	88		102		0.86
	cell control	**100**		**100**		**1**
AgNP#2	80	60	19.5	20	16.2	3.03
	60	48	[18.9–25.6]	13	[13.8–18.7]	3.61
	40	44		11		4.06
	30	39		12		3.41
	20	**48**		**19**		2.53
	15	**73**		**60**		1.23
	10	80		73		**1.09**
	7.5	97		94		1.03
	cell control	**100**		**100**		**1**
AgNP#3	80	**44**	72.2	10	39.4	4.39
	60	**59**	[38.9–76.3]	29	[35.7–50.1]	2.03
	40	68		**47**		1.44
	30	97		**100**		**0.97**
	20	109		98		1.11
	15	106		94		1.13
	10	103		100		1.03
	7.5	102		100		1.02
	cell control	**100**		**100**		**1**
AgNP#4	43	36	7.6	11	4.8	3.45
	33	38	[6.5–7.8]	10	[4.8–5.1]	3.88
	22	39		9		4.06
	16	31		8		3.66
	11	44		8		5.38
	8	**48**		10		4.79
	5.5	**57**		**26**		2.22
	4	91		**81**		**1.12**
	cell control	**100**		**100**		**1**

Table 5
The CC_{50} values for MA-104 cells in MTT and CV tests and IMA of AgNPs.

Sample	MTT CC_{50}, μg/mL	CV CC_{50}, μg/mL	Non-cytotoxic concentrations by IMA, μg/mL
AgNP#1	19.1 [18.5–19.3]	17.6 [15.6–18.0]	15.0
AgNP#2	19.5 [18.9–25.6]	16.2 [13.8–18.7]	10.0
AgNP#3	72.2 [38.9–76.3]	39.4 [35.7–50.1]	30.0
AgNP#4	7.6 [6.5–7.8]	4.8 [4.8–5.1]	4.0

factor is the electrostatic stability factor, which ensures the repulsion of similarly charged particles and prevents their aggregation. As can be seen from Fig. 6b, the largest absolute values of the zeta potential were measured for AgNP#3 and AgNP#1, and accordingly, they demonstrated relatively high stability (Table 3). For AgNP#3, a micelle with a silver nanoparticle stabilized by tannin can be described as a structure where the silver nanoparticle (Ag) forms the core and the tannin molecules (polyphenolic compounds) surround it, acting as stabilizers through adsorption. Tannin molecules have multiple hydroxyl (–OH) groups, which can interact with the silver surface through hydrogen bonding or coordination bonds, leading to stabilization [41–44]. The hydroxyl groups (–OH) of tannin molecules coordinate with the silver atoms on the nanoparticle surface. This interaction can be described as a type of ligand–metal coordination, where the lone pairs of electrons on the oxygen atoms of the hydroxyl groups are donated to the silver atoms, forming a stable bond. Unlike covalent bonds, coordination bonds involve the sharing of lone pairs from the oxygen atoms of hydroxyl groups with the silver atoms. These bonds are strong enough to anchor the tannin molecules onto the nanoparticle surface, providing a stabilizing layer. Upon adsorption, some of the hydroxyl groups in tannin may undergo ionization, releasing protons (H^+) into the surrounding solution and leaving behind negatively charged oxygen atoms (O^-) on the tannin molecules. This process imparts a negative charge to the nanoparticle surface, which contributes to the overall negative zeta potential of the colloidal system. For other synthesized samples, stabilization and formation of a negative surface charge occurs according to a similar mechanism with the participation of flavonoids and other active compounds indicated in the Table 1. The negative charge aids in the electrostatic repulsion between nanoparticles, preventing aggregation.

The UV–Vis spectroscopy data for AgNPs can give indirect information on the size and distribution of the nanoparticles in the dispersions based on the position and shape of the surface plasmon resonance (SPR) peaks [45–49]. For AgNPs, the SPR peak can give an approximation of the nanoparticle size. For small AgNPs (10–100 nm), the SPR peak wavelength increases as the particle size increases. Upon the typical conditions (spherical, well-dispersed silver nanoparticles in water), the following rough estimates can be used: for nanoparticles with a SPR peak around 400–420 nm the particle size is typically in the range of 20–40 nm, for nanoparticles with a SPR peak around 450–470 nm: the particle size is typically larger, around 50–70 nm and for nanoparticles

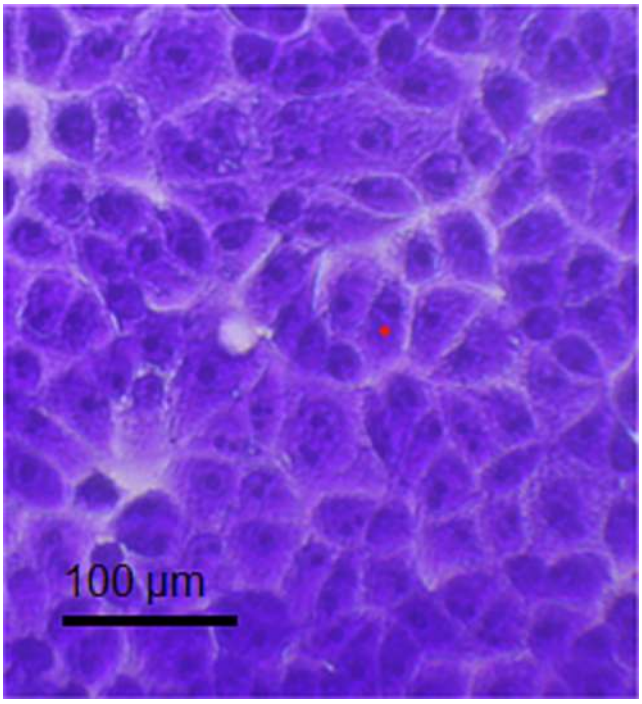

Fig. 8. Image of MA104 cell culture, treated by AgNP#3, in the field of view of a light microscope, stained with crystal violet (magnification x400).

with a SPR peak at shorter wavelengths (e.g., 352 nm) the particle size is generally smaller, possibly in the range of 5–10 nm. The examined silver nanoparticles exhibited a characteristic SPR band in the UV–Vis spectrum (Fig. 7). A broader SPR peak usually indicates a wider size distribution or the presence of polydisperse nanoparticles and a narrow and sharp peak suggests a more monodisperse size distribution. The main peak at 412 nm noted for AgNP#3 (Fig. 7) suggested relatively small silver nanoparticles with an approximate size of 20–30 nm and the small peak at 527 nm could indicate the presence of larger nanoparticles or possibly some degree of agglomeration, which was consistent with the size distribution determined by TEM data.

The broad peak at 462 nm noticed for AgNP#1 suggested a larger average particle size compared to AgNP#3, as the SPR peak is red-shifted. The shoulder at 406 nm could indicate a secondary population of smaller particles within the sample or some inhomogeneity in particle size. The peak at 352 nm observed for AgNP#2 also indicated small nanoparticles and the medium peak at 400 nm suggested a secondary population of slightly larger nanoparticles, possibly indicating a bimodal distribution or polydispersity in the sample. For AgNP#4, a narrow peak at 400 nm was observed, which indicated relatively small and monodisperse distribution of silver nanoparticles. A low intensity of this peak was due to smaller concentration of nanoparticles in comparison with another AgNP preparations.

3.4. Sedimentation and aggregation analysis of the AgNP suspensions

The stability of the AgNP samples was evaluated based on the light transmission and backscattering (Figs. S3–S6) curves as well as the calculated values of TSI (Table 3). The light scattering curves show an increase in scattering over time, which can be associated with an increase in the size of the particles due to their aggregation. According to the Rayleigh's law, scattering of light reflected from the colloidal particles occurs in all directions with the same wavelength as the original radiation and its intensity is proportional to the numerical concentration of particles and the square of the particle volume [50–52].

In the case of aggregation of AgNPs, both of these parameters in the system changed, that is, two processes affecting scattering occurred simultaneously – an increase in the particles size and a simultaneous decrease in their numerical concentration (Figs. S3–S6). In turn, sedimentation is related to the aggregation degree. When the size of particles increases, they can settle due to gravity. In this case, in the left part of the graph, which corresponds to the bottom of the cuvette (see scheme in Fig. S2), an increase in the intensity of scattering will be already observed due to the increase in the numerical concentration of the particles that form the sediment. Such an increase in backscattering in the area of the bottom of the measurement bottle was observed for the all samples of AgNP (Figs. S3–S6).

After 3 days, the highest TSI was observed for the AgNP#2 sample, which indicated the fastest sedimentation of the AgNP aggregates. In turn, the lowest TSI values were observed for the AgNP#1, AgNP#3 and AgNP#4 sample, which indicated their relatively high stability. Various electrolytes affected stability of all synthesized samples. Electrolytes can be divided into indifferent (which do not affect the surface charge) and

Table 6
The results of genotoxicity studies of AgNPs *in vitro*.

CONTROL/ Nanopreparation	Average indicator of genotoxicity for two replicates, I_{DNA}	Conclusion regarding the genotoxicity of AgNPs
NEGATIVE CONTROL	0.402 ± 0.002	not genotoxic
POSITIVE CONTROL	1.964 ± 0.001	genotoxic
AgNP#1	0.408 ± 0.002	not genotoxic
AgNP#2	0.405 ± 0.001	not genotoxic
AgNP#3	0.409 ± 0.001	not genotoxic
AgNP#4	0.408 ± 0.002	not genotoxic

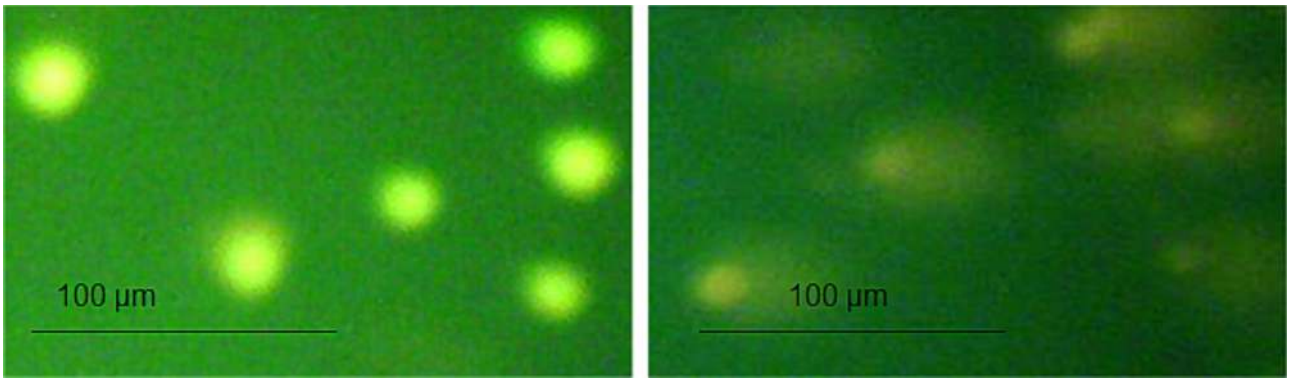

Fig. 9. Image of the "DNA Comet" in the field of view of the microscope, (magnification of x400). A-There is no genotoxic effect under the influence of the studied silver nanoparticles (AgNP#4). DNA of comets 0 and 1 type. B – Genotoxic effect in positive control (N-nitrosomethylurea). DNA of comets of 3,4 type.

potential-determining (which affect the charge on the surface of colloidal particles). Both types of electrolytes affect the value of the zeta potential, that is, the electrostatic stability factor, but by different mechanisms. In the presence of 0.1 M NaCl, 0.1 M $CaCl_2$, or 0.1 M $AlCl_3$, the aggregation and sedimentation in the systems were significantly increased (Figs. S3–S6, Table 3). This can be explained by the presence of monovalent (Na^+), divalent (Ca^{2+}), and trivalent (Al^{3+}) cations in the electric double layer area, which leads to reduction in the absolute values of negative zeta potential. In the presence of triply charged cations, the phenomenon of surface recharging according to Stern is observed, i.e., due to strong specific adsorption of ions Al^{3+} in super-equivalent quantities, the charge on the slipping plane changes from negative to positive (Table 3). When NaOH concentration was increased (i.e., the pH value was higher), the absolute value of negative zeta potential increased and the investigated systems were more stable. In turn, when the concentration of HCl increases (the pH value was more acidic), the stability decreased gradually because the absolute values of negative zeta potential of AgNPs were reduced.

3.5. Cytotoxicity of AgNPs

The obtained results of cytotoxicity tests of the AgNPs samples are shown in Table 4.

For the AgNP#3 and AgNP#4 samples, the CC_{50} indicator in the MTT assay was almost twice as high as in the crystal violet assay, which indicated toxic energy stress of cells in contact with the selected AgNP samples. Table 5 presents the non-toxic concentration according to IMA, that is, the concentration when the IMA values of cells are practically identical or close to the IMA value of control cells equal to 1.0 [0.98–1.06].

For the AgNP#3 sample, the cytotoxic stress effect was accompanied by a significant increase in the IMA, which reached the level of maximum values – up to 6.0. According to the principle of increasing cytotoxicity, the samples can be grouped as follows: AgNP#4 > AgNP#2 > AgNP#1 > AgNP#3. Thus, the non-cytotoxic concentrations of the investigated nanopreparations were (μg/mL for the metal): AgNP#1–15 μg/mL; AgNP#2–10 μg/ml; AgNP#3–30 μg/mL; AgNP#4–4 μg/mL. Fig. 8 shows an image of culture cells MA104 without cytotoxic effect of AgNP#3.

3.6. Genotoxicity of AgNPs

The essence of the Comet assay method is to register differences in the electrophoretic mobility of DNA and its fragments of lysed cells in a constant electrical field. DNA breaks disrupt the structural organization of chromatin which leads to the relaxation of the DNA macromolecule and the formation of its fragments. Alkaline treatment of preparations of lysed cells causes the unravelling of the DNA duplex and allows individual strands to migrate independently in the electrical field. At the same time the DNA migrates to the anode, forming an electrophoretic trace resembling a 'comet tail', the parameters of which depend on the level of damage to the DNA under test. The image of the obtained 'DNA comet' is given in Fig. 9.

The results of genotoxicity studies were also summarized in Table 6. The Comet assay showed the absence of genotoxic effect of the investigated AgNPs. The synthesized AgNPs had no genotoxic effect on eukaryotic cells. Therefore, the entry of such AgNPs into the body of humans or animals will not cause damage to their genetic apparatus.

Based on these results it can be stated that the synthesized silver nanoparticles are biosafe. The obtained data are agreed with the literature reports on eco-friendly silver nanoparticles obtained using plant extracts, i.e., extracts from outer peels of two varieties of *Ipomoea batatas* (L.) Lam., *Aloe vera* and eucalyptus leaf [24,26,27]'.

4. Conclusions

AgNPs were synthesized using 'green' methods to find appropriate, biosafe and stable, additives for hydrogel composites intended for the agro-industrial purposes. The influence of the synthesis procedure on the particle size distribution of AgNPs, their crystalline structure, aggregation and ecotoxicity was determined.

The crystal structure of synthesized silver nanoparticles characterized by XRD and HRTEM crystallization referred to functionally centered cubic, however, for AgNP#1 d-spacing was larger than typical values for the FCC silver, which could be associated with the presence of different phase of silver. During SEM and TEM analyses, for the samples of AgNP#1, AgNP#2 and AgNP#3, mainly individual, spherical nanosilver particles were observed, while for AgNP#4, the aggregates of irregular shape were noted. Sedimentation occurring in the aqueous AgNP dispersions depended significantly on the method of their preparation and the presence of electrolytes (NaCl, $CaCl_2$, $AlCl_3$). For the aqueous AgNPs dispersions without electrolytes, the stability was satisfactory, but in the presence of one, two, and three charged cations, the stability was sharply reduced due to the compression of the electric double layer and the reduction of the electrostatic repulsion between the nanoparticles. The cytotoxicity tests indicated that non-cytotoxic concentrations of the investigated nanoparticles were as follows: AgNP#1–15 μg/ml; AgNP#2–10 μg/ml; AgNP#3–30 μg/mL; AgNP#4–4 μg/mL. Furthermore, the 'Comet assay' showed no genotoxic effect of the investigated AgNPs on eukaryotic cells.

Based on the presented results, the synthesized 'green' nanoparticles can be considered as suitable for incorporation into the structure of hydrogel composites planned as intelligent soil conditioners.

CRediT authorship contribution statement

Svitlana Dybkova: Writing – original draft, Methodology, Investigation, Data curation, Conceptualization. **Olena Goncharuk:** Writing – review & editing, Writing – original draft, Supervision, Project administration, Funding acquisition. **Liudmyla Rieznichenko:** Investigation. **Konrad Terpiłowski:** Validation, Resources, Investigation. **Larysa Borysenko:** Investigation. **Tamara Gruzina:** Investigation. **Kateryna Dybkova:** Methodology, Investigation. **Katarzyna Szewczuk-Karpisz:** Writing – review & editing, Resources, Funding acquisition.

Declaration of competing interest

The authors declare that they have no known competing financial interests or personal relationships that could have appeared to influence the work reported in this paper.

Acknowledgements

The authors, S. Dybkova and O. Goncharuk, are grateful for the financial support by Polish Academy of Sciences and U.S. National Academy of Sciences (Agreement No. PAN.BFB.S.BWZ.331.022.2023 'Biocompatible hybrid hydrogels with functional inorganic fillers for strengthening of plant vegetation').

Appendix A. Supplementary data

Supplementary data to this article can be found online at https://doi.org/10.1016/j.molliq.2024.126319.

Data availability

Data will be made available on request.

References

[1] K.A. Abd-Elsalam, Silver nanomaterials for agri-food applications nanobiotechnology for plant protection. Nanobiotechnology for Plant Protection, Elsevier, 2021.
[2] M. Ghorbanpour, S.A. Wani, Advances in phytonanotechnology from synthesis to application. From Synthesis to Application, Academic Press, 2019.
[3] A. Shelar, S.H. Nile, A.V. Singh, D. Rothenstein, J. Bill, J. Xiao, M. Chaskar, G. Kai, R. Patil, Recent advances in nano-enabled seed treatment strategies for sustainable agriculture: challenges, risk assessment, and future perspectives, Nano-Micro Lett. 15 (2023) 54, https://doi.org/10.1007/s40820-023-01025-5.
[4] O. Naderi, M. Nyman, M. Amiri, R. Sadeghi, Synthesis and characterization of silver nanoparticles in aqueous solutions of surface active imidazolium-based ionic liquids and traditional surfactants SDS and DTAB, J. Mol. Liq. 273 (2019) 645–652, https://doi.org/10.1016/j.molliq.2018.10.046.
[5] N.P.U. Nguyen, N.T. Dang, L. Doan, T.T.H. Nguyen, Synthesis of silver nanoparticles: from conventional to 'modern' methods – a review, Processes 11 (2023) 2617, https://doi.org/10.3390/pr11092617.
[6] S. Iravani, H. Korbekandi, S.V. Mirmohammadi, B. Zolfaghari, Synthesis of silver nanoparticles: chemical, physical and biological methods, Res. Pharm. Sci. 9 (6) (2014) 385–406.
[7] A. Dhaka, S.C. Mali, Sh. Sharma, R. Trivedi, A review on biological synthesis of silver nanoparticles and their potential applications, Result. Chem. 6 (2023) 101108, https://doi.org/10.1016/j.rechem.2023.101108.
[8] T. Mustapha, N. Misni, N.R. Ithnin, A.M. Daskum, N.Z. Unyah, A review on plants and microorganisms mediated synthesis of silver nanoparticles, role of plants metabolites and applications, Int. J. Environ. Res. Public Health 19 (2) (2022) 674, https://doi.org/10.3390/ijerph19020674.
[9] N. Basavegowda, B. Malakar, T.K. Divya, K.N. Beeregowda, L. Padmanabhan, D. Rangappa, S.L. Iconaru, C.S. Ciobanu, Synthesis of plant mediated gold nanoparticles using flower extracts of Carthamus Tintorius L. (safflower) and evaluation of their biological activities, Digest J. Nanomater. Biostruct. 7 (3) (2012) 1289–1295.
[10] N. Basavegowda, G.D. Kumar, B. Tyliszczak, Z. Wzorek, A. Sobczak-Kupiec, One-step synthesis of highly-biocompatibile spherical gold nanoparticles using Artocarpus heteophyllus Lam. (jackfruit) fruit extract and its effect on pathogens, Ann. Agric. Environ. Med. 22 (1) (2015) 84–89, https://doi.org/10.5604/12321966.1141374.
[11] S. Shankar, A.N. Murthy, P. Rachitha, V.B. Raghavendra, S. Ninharaju, A. Chinnathambi, B.S.A. Alharbi, N. Basavegowda, B. Kathirvel, A. Pugazhendhi, Biosynthesis of silk sericin conjugated magnesium oxide nanoparticles for its antioxidant, antiaging, and antibiofilm activities, Environ. Res. 223 (6) (2023) 115421, https://doi.org/10.1016/j.envres.2023.115421.
[12] D. Khedkar, Effects of silver nanoparticles synthesized from rare medicinal plant Radermacheraxylocarpa (Roxb.) K Schumandchlorophyll content on seed germination in Brassica juncea and Vignaradiata, Res. Rev. Biotechnol. Biosci. 7 (2020) 89–103, https://doi.org/10.5281/zenodo.4308462.
[13] M. Hatami, M. Ghorbanpour, Effect of nanosilver on physiological performance of pelargonium plants exposed to dark storage, J. Hort. Res. 21 (2013) 15–20, https://doi.org/10.2478/johr-2013-0003.
[14] T.H. Phong, T. Hieu, H.T. Tung, Silver nanoparticles: a positive factor for in vitro flowering and fruiting of purple passion fruit (Passiflora edulis Sim f. edulis), Plant Cell Tiss. Organ Cult. 151 (2022) 401–412, https://doi.org/10.1007/s11240-022-02361-x.
[15] G.B. Shelar, A.M. Chavan, Myco-synthesis of silver nanoparticles from Trichoderma harzianum and its impact on germination status of oil seed, Biolife 3 (1) (2015) 109–113.
[16] P. Sharma, D. Bhatt, M.G.H. Zaidi, P.P. Saradhi, P.K. Khanna, S. Arora, Silver nanoparticle-mediated enhancement in growth and antioxidant status of *Brassica juncea*, Appl. Biochem. Biotechnol. 167 (8) (2012) 2225–2233, https://doi.org/10.1007/s12010-012-9759-8.
[17] M.S. Sadak, Impact of silver nanoparticles on plant growth, some biochemical aspects, and yield of fenugreek plant (*Trigonella foenumgraecum*), Bullet. National Res. Centre 43 (2019) 38, https://doi.org/10.1186/s42269-019-0077-y.
[18] C. Vannini, G. Domingo, E. Onelli, B. Prinsi, M. Marsoni, L. Espen, M. Bracale, Morphological and proteomic responses of Eruca sativa exposed to silver nanoparticles or silver nitrate, PlosOne 8 (7) (2013) e68752.
[19] F. Abasi, N.I. Raja, Z.U.R. Mashwani, M.S. Amjad, M. Ehsan, N. Mustafa, M. Haroon, J. Proćków, Biogenic silver nanoparticles as a stress alleviator in plants: a mechanistic overview, Molecules 27 (11) (2022) 3378, https://doi.org/10.3390/molecules27113378.
[20] M. Ihtisham, A. Noori, S. Yadav, M. Sarraf, P. Kumari, M. Brestic, M. Imran, F. Jiang, X. Yan, A. Rastogi, Silver nanoparticle's toxicological effects and phytoremediation, Nanomater. (Basel) 11 (9) (2021) 2164, https://doi.org/10.3390/nano11092164.
[21] R. Barrena, E. Casals, J. Colon, X. Font, A. Sánchez, Evaluation of the ecotoxicity of model nanoparticles, Chemosphere 75 (7) (2009) 850–857.
[22] R. Kaveh, Y.S. Li, S. Ranjbar, R. Tehrani, C.L. Brueck, B.V. Aken, Changes in Arabidopsis thaliana gene expression in response to silver nanoparticles and silver ions, Environ. Sci. Technol. 47 (18) (2013) 10637–10644, https://doi.org/10.1021/es402209w.
[23] ISO 10993 - 5:2009. Biological evaluation of medical devices - Part 5: Test for in vitro cytotoxicity. The standard was last reviewed and confirmed in 2022.
[24] G. Das, J.K. Patra, N. Basavegowda, C.N. Vishnuprasad, H.S. Shin, Comparative study on antidiabetic, cytotoxicity, antioxidant and antibacterial properties of biosynthesized silver nanoparticles using outer peels of two varieties of *Ipomoea batatas* (L.) Lam, Int. J. Nanomedicine. 14 (2019) 4741–4754, https://doi.org/10.2147/IJN.S210517.
[25] P.L. Olive, The comet assay: an overview of techniques, Method Mol. Biol. 203 (2002) 179–194.
[26] S.P. Chandran, M. Chaudhary, R. Pasricha, A. Ahmad, M. Sastry, Synthesis of gold nanotriangles and silver nanoparticles using *aloe vera* plant extract, Biotechnol. Prog. 22 (2006) 577–583, https://doi.org/10.1021/bp0501423.
[27] Y.-Y. Mo, Y.-K. Tang, S.-Y. Wang, J.-M. Lin, H.-B. Zhang, D.-Y. Luo, Green synthesis of silver nanoparticles using eucalyptus leaf extract, Mater. Lett. 144 (2015) 165–167, https://doi.org/10.1016/j.matlet.2015.01.004.
[28] S. Surbhi, A. Kumar, S. Singh, P. Kumari, P. Rasane, Eucalyptus: phytochemical composition, extraction methods and food and medicinal applications, Adv. Tradition. Med. 23 (2023) 369–380, https://doi.org/10.1007/s13596-021-00582-7.
[29] B. Salehi, S. Albayrak, H. Antolak, D. Kręgiel, E. Pawlikowska, M. Sharifi-Rad, Y. Uprety, P.V. Tsouh Fokou, Z. Yousef, Z. Amiruddin Zakaria, E.M. Varoni, F. Sharopov, N. Martins, M. Iriti, J. Sharifi-Rad, Aloe genus plants: from farm to food applications and phytopharmacotherapy, Int. J. Mol. Sci. 19 (9) (2018) 2843, https://doi.org/10.3390/ijms19092843.
[30] JCPDS Database, International Center for Diffraction Data, PA, 2001.
[31] R. Jenkins, R.L. Snyder, Introduction to X-Ray Powder Diffractometry, John Wiley & Sons Inc, New York, 1996.
[32] Malvern Instruments [homepage on the Internet], 2017. Available from: https://www.malvern.com.
[33] M. Wiśniewska, K. Terpiłowski, S. Perez Huertas, I. Ostolska, K. Szewczuk-Karpisz, O. Goncharuk, Turbidimetric studies of colloidal silica/aqueous solution system stability, Surf. Innov. 5 (2017) 138–146, https://doi.org/10.1680/jsuin.17.00018.
[34] A.R. Collins, The comet assay for DNA damage and repair: principles, applications and limitations, Mol. Biotechnol. 26 (3) (2004) 249–261.
[35] V.V. Didenko, Methods in molecular biology. In situ detection of DNA damage, Method, Protocol. 203 (2002) 299.
[36] B.D. Cullity, S.R. Stock, Elements of X-ray diffraction, Pearson (2014).
[37] J. Hentschel, S. Kumar, Unusual crystal structures in nanomaterials, J. Nanomater. (2008).
[38] Y. Sun, Y. Xia, Shape-controlled synthesis of metal nanocrystals, Science 298 (5601) (2002) 2176–2179, https://doi.org/10.1021/jacs.5b04641.
[39] B.J. Berne, R. Pecora, Dynamic Light Scattering, Courier Dover Publications, 2000.
[40] K. Szewczuk-Karpisz, G. Rzepa, T. Bajda, M. Wiśniewska, T. Urban, S. Kukowska, A. Tomczyk, K. Grygorczuk-Płaneta, B. Kondracki, Aggregation mechanism of natural schwertmannite particles covered with two-component layers of high molecular weight tackifier and trace metal ions, J. Mol. Liq. 368 (5) (2022) 120746, https://doi.org/10.1016/j.molliq.2022.120746.
[41] S. Prabhu, E.K. Poulose, Silver nanoparticles: mechanism of antimicrobial action, synthesis, medical applications, and toxicity effects, Int. Nano Lett. 2 (1) (2012) 1–10, https://doi.org/10.1186/2228-5326-2-32.
[42] H. Wang, Y. Qiao, S. Jiang, Y. Liu, S. Gao, Biosynthesis of silver nanoparticles using tannic acid and its antibacterial mechanism under dual UV-visible radiation, J. Mol. Struct. 1114 (2016) 1–7.
[43] A. Gul, R. Gul, M. Zaman, S. Noreen, N.U. Rehman, S. Waseem, Tannin stabilized silver nanoparticles: green synthesis, characterization, and antibacterial activity, J. Nanomater. 2021 (2021).
[44] R. Chandrasekaran, S.A. Yadav, A. Mukherjee, Tannin-mediated synthesis of silver nanoparticles and their bactericidal properties, Mater. Today: Proc. 26 (2020) 2577–2581.
[45] K.L. Kelly, E. Coronado, L.L. Zhao, G.C. Schatz, The optical properties of metal nanoparticles: the influence of size, shape, and dielectric environment, J. Phys. Chem. B 107 (3) (2003) 668–677, https://doi.org/10.1021/jp026731y.
[46] W. Haiss, N.T.K. Thanh, J. Aveyard, D.G. Fernig, Determination of size and concentration of gold nanoparticles from UV-vis spectra, Anal. Chem. 79 (11) (2007) 4215–4221, https://doi.org/10.1021/ac0702084.
[47] S. Link, M.A. El-Sayed, Size and temperature dependence of the plasmon absorption of colloidal gold nanoparticles, J. Phys. Chem. B 103 (21) (1999) 4212–4217.
[48] D. Paramelle, A. Sadovoy, S. Gorelik, P. Free, J. Hobley, D.G. Fernig, A rapid method to estimate the concentration of citrate capped silver nanoparticles from UV-visible light spectra, Anal. Chem. 86 (2) (2014) 835–843.
[49] C. Noguez, Surface plasmons on metal nanoparticles: the influence of shape and physical environment, J. Phys. Chem. C 111 (10) (2007) 3806–3819.
[50] H. Yin, P.S. Casey, Effects of particle size and charge on the UV-visible extinction of colloidal silver nanoparticles in aqueous solution, J. Colloid Interface Sci. 322 (2) (2008) 394–400.
[51] E.J.W. Verwey, J.T.G. Overbeek, Theory of the Stability of Lyophobic Colloids, Courier Corporation, 1999.
[52] J. Lyklema, Fundamentals of Interface and Colloid Science, Academic Press, 2005.